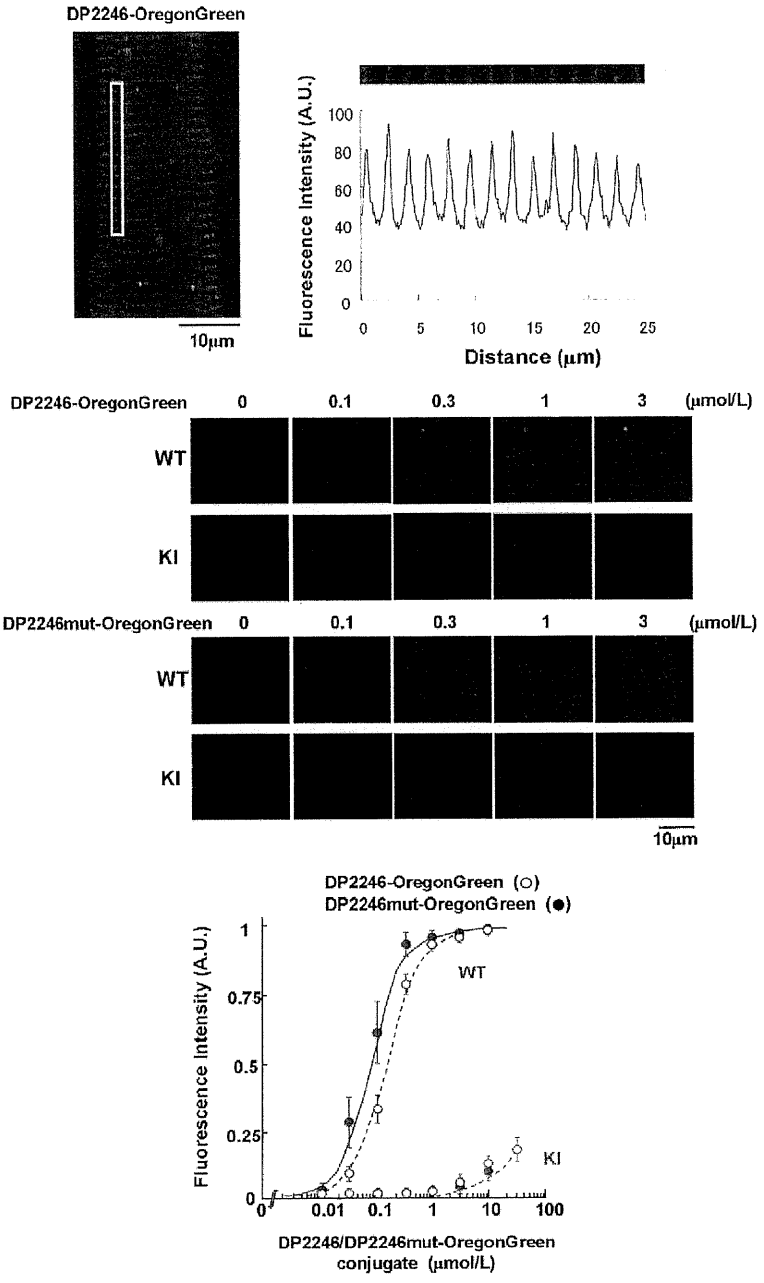

Figure 6. Localization and the characteristics of DP2246 binding to the cellular components (sarcoplasmic reticulum in situ) of saponin-permeabilized wild-type (WT) and knockin (KI) cardiomyocytes. **Top**, The DP2246, fluorescently labeled with Oregon Green 514 (Molecular Probes, OR), was delivered into the cardiomyocytes. **Middle**, Representative images of Oregon Green–labeled DP2246 or DP2246mut in WT and KI cardiomyocytes. **Bottom**, The plot of the intensity of the fluorescence along the sarcomeres as a function of the concentration of DP2246 (open circle)/DP2246mut (closed circle)–Oregon Green. Data represent mean±SE of 4 to 5 cells from 3 to 4 hearts.

was no significant difference in the amount of RyR2-bound FKBP12.6 between WT and knockin mice.

Discussion

A considerable body of evidence accumulated over recent years suggests that mutation-linked RyR2 defects cause SR Ca^{2+} leak, which triggers delayed afterdepolarization and ultimately leads to CPVT.[2] Recently, several groups developed knockin mouse models harboring several different point mutations of RyR2 corresponding to the CPVT mutations of human patients (R4496C,[15] R176Q,[16] and R2474S[13,17]) and have shown that these mutations produce phenotypes of CPVT similar to those of human patients. The fact that these point mutations produce almost identical phenotypes of CPVT regardless of their locations within the RyR2 suggests that a mutation introduced into a particular location produces a global impact on the channel regulation mechanism (eg, by mediation of defective interdomain interaction in its local area first and then by coupled global conformational change of the RyR2). However, little work has been done in this new area of exploration.

The important new concept deduced from the present study, summarized in Figure 8, is that the S2246L mutation that is introduced into the region of RyR2, different from that of the aforementioned R2474S mutation, causes an abnormally tight interaction (zipping) of a new interacting domain pair (namely, 2 subdomains: 2246 domain/K201-binding domain [2114 to 2149]) located in the central domain and that this intersubdomain interaction is coupled

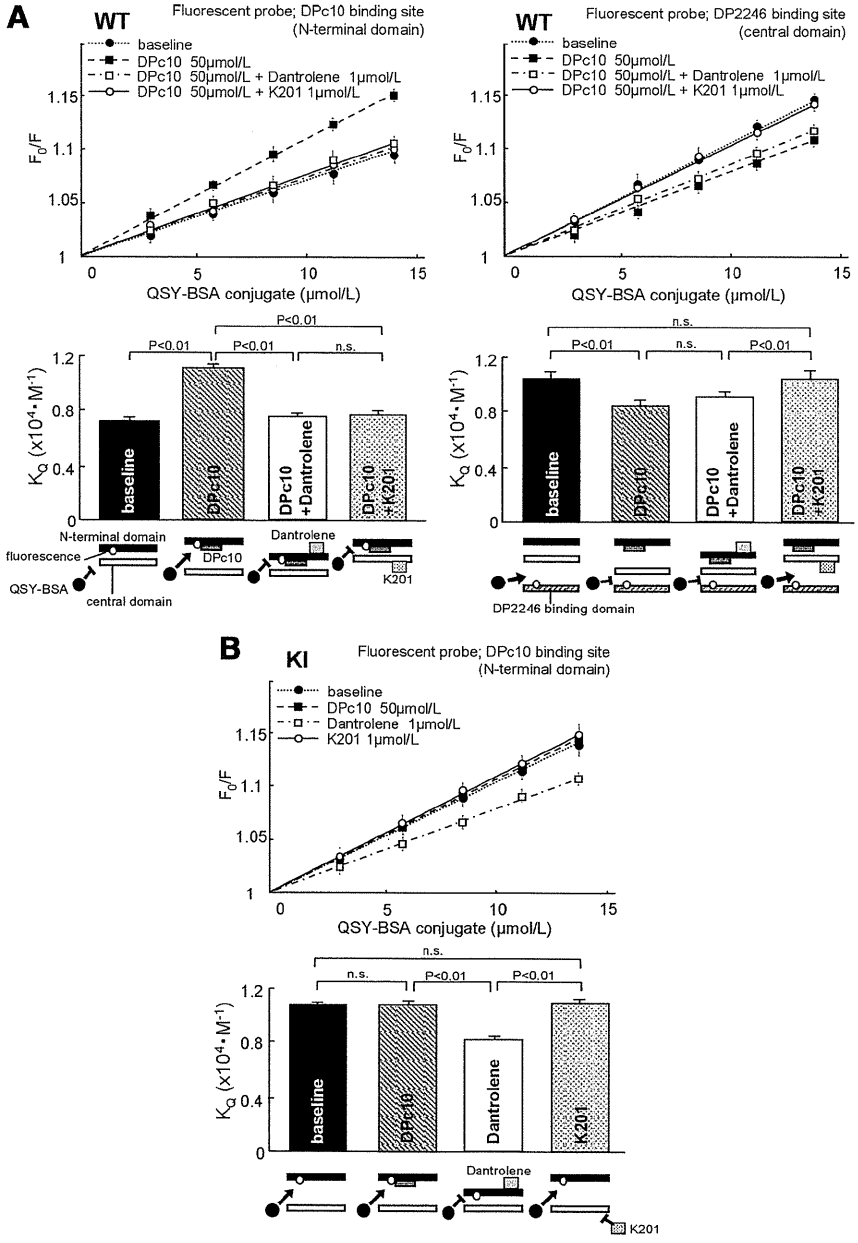

Figure 7. Determination of the mode of interdomain interactions in the domain switch (interacting pair of the N-terminal and central domains) and in the 2246 domain/K201-binding domain pair of wild-type (WT) and knockin (KI) ryanodine receptors. The slope of the Stern-Volmer plots of the fluorescence quenching data with QSY–bovine serum albumin (QSY-BSA) (K_Q) corresponds with the accessibility of the quencher and serves as a measure of the magnitude of domain unzipping. Effect of DPc10 or DP2246 on the K_Q in WT (**A**) or KI (**B**) sarcoplasmic reticulum is shown; methylcoumarin acetamido labeling was done in a site-directed manner with the use of DPc10 or DP2246 as a carrier. The data are shown as mean±SE of 5 to 6 experiments with 3 to 4 SR preparations from 30 to 40 mouse hearts.

with unzipping of the domain switch in an allosteric manner. Thus, the S2246L mutation ends up with aberrant unzipping of the domain switch, then produces the same type of channel dysfunction and CPVT phenotypes as those produced by the R2474S mutation. This concept is supported by the following pieces of evidence. First, DP2246, a peptide corresponding to the 2246 domain (2232 to 2266), was found to bind with the 2114 to 2149 region of RyR2, the previously identified K201-binding domain.[11] This suggests that there is an interaction between the 2246 domain and the K201-binding domain. As shown in the experiment with WT SR, the binding affinity of DP2246mut to RyR2 was much higher than that of DP2246, suggesting that the mutation induces a tight zipping of this interacting subdomain pair. In support of this view, DP2246–Oregon Green was not accessible to its binding site in the knockin cardiomyocytes, although it was accessible in the WT cardiomyocytes. Second, DPc10, the central domain peptide that binds to the N-terminal domain and unzips the domain switch,[9,13] induced domain zipping between the 2246 domain and its partner K201-binding domain, indicating again that reciprocal conformational changes in the 2 regions are tightly coupled. Importantly, in the knockin RyR2, DPc10 was without effect; this is because the domain switch had already been unzipped owing to the allosteric coupling with the tightly zipped 2246 domain/K201-binding domain pair. Third, the S2246L mutation produced CPVT phenotypes identical to those produced by the R2474S mutation. Thus, the threshold of SR Ca^{2+} load for channel activation (determined as increased Ca^{2+} sparks) was markedly reduced in both the S2246L and the R2474S knockin cardiomyocytes. The

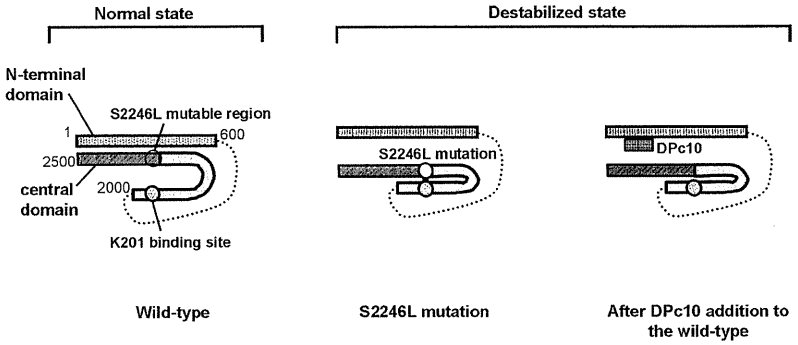

Figure 8. Hypothetical model showing how catecholaminergic polymorphic ventricular tachycardia–associated mutation causes a drastic change in the channel function by mediation of defective interdomain interactions within ryanodine receptor (RyR2). In the "normal state" of RyR2, tight interaction between the N-terminal domain and the central domain (zipped domain switch) is coupled with a loose interaction (unzipping) between the 2 subdomains of the central domain (the 2246 domain [S2246L mutable region] and the K201-binding domain), then the closed state of the channel is maintained. In the "destabilized state," the S2246L mutation in the 2246 domain induces an abnormally tight interaction of the S2246 domain/K201-binding domain pair. This produces domain unzipping of the N-terminal domain/central domain pair (the domain switch), and erroneous activation of the channel results in diastolic Ca^{2+} leak. Addition of DPc10, which interferes with a tight interaction between the N-terminal and central domains, to the wild-type RyR2 produces domain unzipping of the domain switch, mimicking the situation caused by catecholaminergic polymorphic ventricular tachycardia mutation (R2474S, S2246L).

same phenotype could be reproduced in the WT cardiomyocytes by experimentally unzipping the domain switch with DPc10. Thus, the present study provides preliminary evidence for a more generalized hypothesis that critical mutation in a particular area of the RyR2 causes defective interdomain interaction in its vicinity, which is then linked to a global conformational change that leads to channel activation by mediation of the allosteric conformational coupling mechanism. This would account for the fact that most of all of the CPVT mutations in different locations of RyR2 investigated in transgenic mouse models of CPVT have produced a virtually identical type of channel disorder and CPVT phenotypes.[13,15–17] One of the 3 mutations investigated in the literature of the transgenic mouse models of CPVT, R4496C,[15] is localized in the "I" domain (3772 to 4610), whose steady interaction with the transmembrane channel region seems to play an important role in normal channel regulation.[21,22] On the basis of this new expanded concept, we postulated that the I domain/channel domain interaction is coupled with the conformational changes in the domain switch and the 2246 domain/K201-binding domain pair, and mutation-caused defective interdomain interaction in any of these regions is transmitted to the channel as a pathogenic signal.

One of the most important aspects in the present study is the finding that dantrolene corrected the defective unzipped state of the domain switch (Figure 7) and then inhibited exercise-induced VT in the S2246L knockin mice (Figure 1). Because the dantrolene binding site is localized in the 600 to 620 residue region of the N-terminal domain of RyR2,[12] this indicates that dantrolene binding to its binding site corrected defective unzipping of the interacting N-terminal domain/central domain pair that had been produced by the S2246L mutation in the 2246 domain. As mentioned above, the mutation in the 2246 domain tightens its interaction with the K201-binding domain, and this local conformational change causes domain unzipping in the domain switch by the mechanism of conformational coupling between these 2 regions. Conversely, dantrolene-mediated correction of aberrant unzipped configuration of the domain switch restores a normal stabilized state of the channel and stops VT, even though the drug produced virtually no effect on the 2246 domain/K201-binding domain interaction. We have shown previously in the canine heart failure model that dantrolene corrects defective unzipping between the N-terminal domain and the central domain to a normal zipped state and prevents the development of heart failure inducible by ventricular pacing.[12] Thus, it appears that defective interdomain interaction of the domain switch is a source mechanism underlying CPVT and heart failure and provides a key target of therapeutic treatment.

Although the R2474S and S2246L mutations produce basically identical impacts on the structure and function of the RyR2 as described above, there are delicate differences in the 2 aspects: (1) the response to PKA phosphorylation and (2) the pharmacological effect of K201. First, we reported previously that the R2474S mutation caused a partial unzipping of the domain switch, and on PKA phosphorylation at Ser2808 of RyR2, the domain switch was unzipped to a "full" extent.[13] The S2246L/+ knockin RyR2, on the other hand, showed a nearly maximal extent of domain unzipping under baseline conditions, accompanied by increased Ca^{2+} spark frequency with reduced SR Ca^{2+} content; consequently, PKA phosphorylation produced no further domain unzipping and hence no further effect on Ca^{2+} spark frequency (Figure 2D). Second, as we demonstrated previously in the studies of a canine heart failure model,[11] K201 binding to its binding domain interfered with the interaction between the K201-binding domain and the 2246 domain and corrected channel dysfunctions of RyR2 of the failing heart. In the R2474S/+ knockin mouse model, K201 as well as dantrolene suppressed PKA phosphorylation-dependent channel activation (H. Uchinoumi, MD, PhD, et al, unpublished data, 2010). In the S2246L/+ knockin mouse model, however, K201 showed no appreciable

corrective effect on both domain switch unzipping and channel activation (Figure 2F), although dantrolene produced the expected effects. These differences, as outlined above, may be accounted for by the fact that the S2246L mutation causes an excessively tight interaction of the K201-binding domain/2246 domain pair, which results in (1) facilitated unzipping of the domain switch by the conformational coupling between the 2 regions and (2) the inaccessibility of the K201-binding domain for the drug binding owing to its tight interaction with the 2246 domain.

Taken together, conformational coupling of different regions of RyR2 may explain the fact that mutations in different areas of the receptor produce a similar phenotype. However, in view of the nonidentical effects of the 2 types of potential therapeutic agents described in this report, differences in the mode of interdomain interaction in those different areas, to which dantrolene and K201 bind, may result in the observed differences in their therapeutic efficacy.

The present studies do not include the potential contribution of CaMKII, although the use of KN-93 could be complicated by off-target effects that are unrelated to CaMKII activity on the basis of similar experience with KN-93 on other ion channels. A further investigation is clearly needed to assess the role of CaMKII in mutation-linked local Ca^{2+} events.

In conclusion, introduction of a human CPVT mutation S2246L into the mouse RyR2 induces aberrant activation of channel gating by forming abnormally tight domain-domain interaction between the 2 subdomains located in the central domain: the S2246L mutable domain (residue 2232 to 2266) and the K201-binding domain (residue 2114 to 2149). This produces a defective domain unzipping between the N-terminal (residue 1 to 600) domain and the central (residue 2000 to 2500) domain owing to the allosteric conformational coupling between the 2 sets of interacting domain pairs. The coupled conformational changes in these regions trigger diastolic Ca^{2+} release and lethal arrhythmia. Dantrolene treatment corrected the defective interdomain interaction and prevented aberrant Ca^{2+} release and CPVT, indicating that correction of the conformational disorder of RyR2 is a new therapeutic strategy for CPVT.

Sources of Funding

This work was supported by grants-in-aid for scientific research from the Ministry of Education in Japan (grants 20390226 to Dr Yano, 20590868 to Dr Yamamoto, 20591805 to Dr Kobayashi), Takeda Science Foundation to Dr Yano, and a grant from the National Heart, Lung, and Blood Institute (HL072841 to Dr Ikemoto). The authors declare no competing financial interests.

Disclosures

None.

References

1. Bers DM. Macromolecular complexes regulating cardiac ryanodine receptor function. *J Mol Cell Cardiol.* 2004;37:417–429.
2. Clusin WT. Calcium and cardiac arrhythmias: DADs, EADs, and alternans. *Crit Rev Clin Lab Sci.* 2003;40:337–375.
3. Thomas NL, Maxwell C, Mukherjee S, Williams AJ. Ryanodine receptor mutations in arrhythmia: the continuing mystery of channel dysfunction. *FEBS Lett.* 2010;584:2153–2160.
4. Ikemoto N, Yamamoto T. Regulation of calcium release by interdomain interaction within ryanodine receptors. *Front Biosci.* 2002;7:d671–d683.
5. Ikemoto N. Intra-molecular domain-domain interaction: a key mechanism for calcium channel regulation of ryanodine receptors. In: Wehrens XHT, Marks AR, eds. *Ryanodine Receptors: Structure, Function and Dysfunction in Clinical Disease.* New York, NY: Springer; 2004:53–65.
6. Yamamoto T, El-Hayek R, Ikemoto N. Postulated role of interdomain interaction within the ryanodine receptor in Ca^{2+} channel regulation. *J Biol Chem.* 2000;275:11618–11625.
7. Liu Z, Wang R, Zhang J, Chen SR, Wagenknecht T. Localization of a disease-associated mutation site in the three-dimensional structure of the cardiac muscle ryanodine receptor. *J Biol Chem.* 2005;280:37941–37947.
8. Wang R, Chen W, Cai S, Zhang J, Bolstad J, Wagenknecht T, Liu Z, Chen SR. Localization of an NH2-terminal disease-causing mutation hot spot to the "clamp" region in the three-dimensional structure of the cardiac ryanodine receptor. *J Biol Chem.* 2007;282:17785–17793.
9. Oda T, Yano M, Yamamoto T, Tokuhisa T, Okuda S, Doi M, Ohkusa T, Ikeda Y, Kobayashi S, Ikemoto N, Matsuzaki M. Defective regulation of interdomain interactions within the ryanodine receptor plays a key role in the pathogenesis of heart failure. *Circulation.* 2005;111:3400–3410.
10. Mochizuki M, Yano M, Oda T, Tateishi H, Kobayashi S, Yamamoto T, Ikeda Y, Ohkusa T, Ikemoto N, Matsuzaki M. Scavenging free radicals by low-dose carvedilol prevents redox-dependent Ca2+ leak via stabilization of ryanodine receptor in heart failure. *J Am Coll Cardiol.* 2007;49:1722–1732.
11. Yamamoto T, Yano M, Xu X, Uchinoumi H, Tateishi H, Mochizuki M, Oda T, Kobayashi S, Ikemoto N, Matsuzaki M. Identification of target domains of the cardiac ryanodine receptor to correct channel disorder in failing hearts. *Circulation.* 2008;117:762–772.
12. Kobayashi S, Yano M, Suetomi T, Ono M, Tateishi H, Mochizuki M, Xu X, Uchinoumi H, Okuda S, Yamamoto T, Koseki N, Kyushiki H, Ikemoto N, Matsuzaki M. Dantrolene, a therapeutic agent for malignant hyperthermia, markedly improves the function of failing cardiomyocytes by stabilizing inter-domain interactions within the ryanodine receptor. *J Am Coll Cardiol.* 2009;53:1993–2005.
13. Uchinoumi H, Yano M, Suetomi T, Ono M, Xu X, Tateishi H, Oda T, Okuda S, Doi M, Kobayashi S, Yamamoto T, Ikeda Y, Ohkusa T, Ikemoto N, Matsuzaki M. Catecholaminergic polymorphic ventricular tachycardia is caused by mutation-linked defective conformational regulation of the ryanodine receptor. *Circ Res.* 2010;106:1413–1424.
14. Kobayashi S, Yano M, Uchinoumi H, Suetomi T, Susa T, Ono M, Xu X, Tateishi H, Oda T, Okuda S, Doi M, Yamamoto T, Matsuzaki M. Dantrolene, a therapeutic agent for malignant hyperthermia, inhibits catecholaminergic polymorphic ventricular tachycardia in a RyR2(R2474S/+) knock-in mouse model. *Circ J.* 2010;74:2579–2584.
15. Cerrone M, Colombi B, Santoro M, di Barletta MR, Scelsi M, Villani L, Napolitano C, Priori SG. Bidirectional ventricular tachycardia and fibrillation elicited in a knock-in mouse model carrier of a mutation in the cardiac ryanodine receptor. *Circ Res.* 2005;96:e77–e82.
16. Kannankeril PJ, Mitchell BM, Goonasekera SA, Chelu MG, Zhang W, Sood S, Kearney DL, Danila CI, De Biasi M, Wehrens XH, Pautler RG, Roden DM, Taffet GE, Dirksen RT, Anderson ME, Hamilton SL. Mice with the R176Q cardiac ryanodine receptor mutation exhibit catecholamine-induced ventricular tachycardia and cardiomyopathy. *Proc Natl Acad Sci U S A.* 2006;103:12179–12184.
17. Lehnart SE, Mongillo M, Bellinger A, Lindegger N, Chen BX, Hsueh W, Reiken S, Wronska A, Drew LJ, Ward CW, Lederer WJ, Kass RS, Morley G, Marks AR. Leaky Ca^{2+} release channel/ryanodine receptor 2 causes seizures and sudden cardiac death in mice. *J Clin Invest.* 2008;118:2230–2245.
18. Yano M, Kobayashi S, Kohno M, Doi M, Tokuhisa T, Okuda S, Suetsugu M, Hisaoka T, Obayashi M, Ohkusa T, Kohno M, Matsuzaki M. FKBP12.6-mediated stabilization of calcium-release channel (ryanodine receptor) as a novel therapeutic strategy against heart failure. *Circulation.* 2003;107:477–484.
19. Marx SO, Reiken S, Hisamatsu Y, Jayaraman T, Burkhoff D, Rosemblit N, Marks AR. PKA phosphorylation dissociates FKBP12.6 from the calcium release channel (ryanodine receptor): defective regulation in failing hearts. *Cell.* 2000;101:365–376.
20. Yano M, Ono K, Ohkusa T, Suetsugu M, Kohno M, Hisaoka T, Kobayashi S, Hisamatsu Y, Yamamoto T, Kohno M, Noguchi N,

Takasawa S, Okamoto H, Matsuzaki M. Altered stoichiometry of FKBP12.6 versus ryanodine receptor as a cause of abnormal Ca(2+) leak through ryanodine receptor in heart failure. *Circulation*. 2000;102: 2131–2136.
21. George CH, Jundi H, Thomas NL, Scoote M, Walters N, Williams AJ, Lai FA. Ryanodine receptor regulation by intramolecular interaction between cytoplasmic and transmembrane domains. *Mol Biol Cell*. 2004; 15:2627–2638.
22. George CH, Jundi H, Walters N, Thomas NL, West RR, Lai FA. Arrhythmogenic mutation-linked defects in ryanodine receptor autoregulation reveal a novel mechanism of Ca2+ release channel dysfunction. *Circ Res*. 2006;98:88–97.

CLINICAL PERSPECTIVE

Catecholaminergic polymorphic ventricular tachycardia (CPVT) is an inherited disease characterized by stress- or exercise-induced polymorphic ventricular tachycardia, frequently leading to sudden cardiac death. A considerable body of evidence accumulated over recent years suggests that mutation-linked cardiac ryanodine receptor defects cause Ca^{2+} leak from sarcoplasmic reticulum, which triggers delayed afterdepolarization and ultimately leads to CPVT. However, the underlying mechanism, by which a single mutation in such a large molecule causes drastic effects on the channel function, remains unresolved. Here we report that introduction of a human CPVT mutation S2246L (serine to leucine mutation at residue 2246) into the mouse ryanodine receptor induces aberrant activation of channel gating by forming an abnormally tight domain-domain interaction between the S2246L mutable domain (residue 2232 to 2266) and the K201-binding domain (residue 2114 to 2149). This produces more global conformational change in the ryanodine receptor: an aberrant domain unzipping between the N-terminal (residue 1 to 600) domain and the central (residue 2000 to 2500) domain owing to the allosteric conformational coupling mechanism. The coupled conformational changes in these local and global interdomain interactions trigger diastolic Ca^{2+} release and lethal arrhythmia. Pharmacological correction of the defective interdomain interactions can stop the aberrant Ca^{2+} release and lethal arrhythmia. These results provide a new pathogenic mechanism of CPVT and a novel therapeutic strategy against CPVT.

Journal of the American College of Cardiology
© 2012 by the American College of Cardiology Foundation
Published by Elsevier Inc.

Vol. 59, No. 9, 2012
ISSN 0735-1097/$36.00
doi:10.1016/j.jacc.2011.10.887

PRE-CLINICAL RESEARCH

Cardiac-Specific Deletion of SOCS-3 Prevents Development of Left Ventricular Remodeling After Acute Myocardial Infarction

Toyoharu Oba, MD,* Hideo Yasukawa, MD, PHD,*† Masahiko Hoshijima, MD, PHD,‡ Ken-ichiro Sasaki, MD, PHD,*† Nobuyoshi Futamata, MD,* Daisuke Fukui, MD,* Kazutoshi Mawatari, MD,* Takanobu Nagata, MD,* Sachiko Kyogoku, MD,* Hideki Ohshima, MD,* Tomoko Minami, MD,* Keiichiro Nakamura, MD, PHD,§ Dongchon Kang, MD, PHD,‖ Toshitaka Yajima, MD, PHD,‡ Kirk U. Knowlton, MD,‡ Tsutomu Imaizumi, MD, PHD*†

Kurume, Japan; and La Jolla, California

Objectives The study investigated the role of myocardial suppressor of cytokine signaling-3 (SOCS3), an intrinsic negative feedback regulator of the *janus* kinase and signal transducer and activator of transcription (JAK-STAT) signaling pathway, in the development of left ventricular (LV) remodeling after acute myocardial infarction (AMI).

Background LV remodeling after AMI results in poor cardiac performance leading to heart failure. Although it has been shown that JAK-STAT–activating cytokines prevent LV remodeling after AMI in animals, little is known about the role of SOCS3 in this process.

Methods Cardiac-specific SOCS3 knockout mice (SOCS3-CKO) were generated and subjected to AMI induced by permanent ligation of the left anterior descending coronary artery.

Results Although the initial infarct size after coronary occlusion measured by triphenyltetrazolium chloride staining was comparable between SOCS3-CKO and control mice, the infarct size 14 days after AMI was remarkably inhibited in SOCS3-CKO, indicating that progression of LV remodeling after AMI was prevented in SOCS3-CKO hearts. Prompt and marked up-regulations of multiple JAK-STAT–activating cytokines including leukemia inhibitory factor and granulocyte colony-stimulating factor (G-CSF) were observed within the heart following AMI. Cardiac-specific SOCS3 deletion enhanced multiple cardioprotective signaling pathways including STAT3, AKT, and extracellular signal-regulated kinase (ERK)-1/2, while inhibiting myocardial apoptosis and fibrosis as well as augmenting antioxidant expression.

Conclusions Enhanced activation of cardioprotective signaling pathways by inhibiting myocardial SOCS3 expression prevented LV remodeling after AMI. Our data suggest that myocardial SOCS3 may be a key molecule in the development of LV remodeling after AMI. (J Am Coll Cardiol 2012;59:838–52) © 2012 by the American College of Cardiology Foundation

Left ventricular (LV) remodeling after acute myocardial infarction (AMI) is characterized by infarct expansion, LV dilation, and fibrosis of viable myocardium (1–3). This adverse LV remodeling depresses cardiac performance, contributes to the development of heart failure, and is an independent determinant of morbidity and mortality after AMI (1–3). Although several major therapeutic advances have been made in the management of AMI, the number of patients with congestive heart failure is increasing; these patients carry a >10-fold increased risk of death (1–3).

From the *Division of Cardiovascular Medicine, Department of Internal Medicine, Kurume University School of Medicine, Kurume, Japan; †Cardiovascular Research Institute, Kurume University, Kurume, Japan; ‡Department of Medicine, University of California, San Diego, La Jolla, California; §Division of Microscopic and Developmental Anatomy, Department of Anatomy, Kurume University School of Medicine, Kurume, Japan; and the ‖Department of Clinical Chemistry and Laboratory Medicine, Kyushu University Graduate School of Medical Sciences, Fukuoka, Japan. This study was supported by Grants-in-Aid for Scientific Research, the Program for Promotion of Fundamental Studies in Health Sciences of the National Institute of Biomedical Innovation (NIBIO); a grant for the Academic Frontier Project from the Ministry of Education, Science, Sports, Culture, and Technology, Japan; Mochida Memorial Foundation; Uehara Memorial Foundation; and Takeda Memorial Foundation. All authors have reported that they have no relationships relevant to the contents of this paper to disclose. Douglas Mann, MD, served as Guest Editor for this article.

Manuscript received September 19, 2011; revised manuscript received October 19, 2011, accepted October 20, 2011.

Accordingly, it is important to elucidate the mechanisms underlying post-infarct LV remodeling and to develop therapeutic strategies that will effectively suppress this adverse process (1,4).

The administration of cytokines such as granulocyte colony-stimulating factor (G-CSF), erythropoietin, interleukin (IL)-11, and leukemia inhibitory factor (LIF) was recently demonstrated to prevent the development of LV remodeling after AMI in animals (5–11). These cytokines activate the *janus* kinase (JAK) and signal transducer and activator of transcription (STAT) pathways, which have protective roles in the development of LV remodeling after AMI (12–16). Although JAK-STAT–activating cytokines prevent LV remodeling after AMI in animals, little is known about the role of a negative feedback regulator for the JAK-STAT signaling pathway in this process.

Suppressor of cytokine signaling (SOCS) family proteins were identified as cytokine-inducible intrinsic inhibitors of cytokine signaling (17,18). We demonstrated previously that SOCS1 and SOCS3 strongly inhibit JAK-STAT–mediated cytokine signaling pathways as pseudosubstrates by interacting with JAK and inhibiting JAK activity (17–19). SOCS3 is induced by JAK-STAT–activating cytokines, including G-CSF, erythropoietin, and LIF, and acts to inhibit their actions (18–20). We previously showed that the forced expression of SOCS3 inhibited cytokine-promoted cardiomyocyte survival in vitro and that cardiac-specific transgenic expression of SOCS3 facilitated coxsackievirus-induced cardiac injury in mice by inhibiting the JAK-STAT signaling pathway (20–22). Thus, SOCS3 is a cytokine-inducible inhibitor of the JAK-STAT pathway that promotes myocardial cell survival. Therefore, we hypothesized that the inhibition of myocardial SOCS3 would prevent LV remodeling after AMI. To test this hypothesis, we generated cardiac-specific SOCS3 knockout mice (SOCS3-CKO) using the Cre recombinase and loxP system (23). We then induced AMI in these mice by permanently ligating the left anterior descending coronary artery, and investigated the role of myocardial SOCS3 in the development of LV remodeling after AMI.

Methods

Generation of SOCS3-CKO. Because SOCS3-deficient mice die during embryonic development as a result of placental defects, the SOCS3 coding region in exon2 was flanked by loxP sites (flox) (Fig. 1A), and we generated SOCS3-flox mice to determine the tissue-specific roles of SOCS3 (23,24). To investigate the role of JAK-STAT signaling and its negative regulator SOCS3 in LV remodeling after AMI, SOCS3-flox mice were bred with α-myosin heavy chain–promoter-driven cardiac-specific Cre recombinase transgenic mice (25). We confirmed that SOCS3 protein was markedly reduced in SOCS3-CKO hearts 6 h after intraperitoneal injection of lipopolysaccharide (LPS) (20 mg/kg) (Fig. 1B).

The mice used in this study were 8- to 10-week-old males in a Balb/c background. All experimental procedures were performed according to the guidelines for experiments in animals established by the Kurume University Animal Care and Treatment Committee for experiments in animals.

Acute myocardial infarction model. Acute myocardial infarction was produced by permanent ligation of the left coronary artery as previously described. To measure infarct size 14 days after AMI, the LV were cut into 3 transverse sections from apex to base. Five-micrometer sections were stained with Mallory-AZAN staining. The extent of fibrosis was measured in 3 sections and the value was expressed as the ratio of Mallory-AZAN–stained area to total LV free wall (5). Evans blue dye and triphenyltetrazolium chloride (TTC) stains were also performed to measure initial infarct size. Area at risk and infarct area were determined by perfusion with 5% Evans blue and consequent incubation with TTC at 3 h after left coronary artery occlusion, as previously described (12).

Western blot analysis. Western blot analysis was performed as described previously (20–22) with the use of antibodies raised against tyrosine-phosphorylated STAT3, serine-phosphorylated STAT3, phosphorylated AKT, phosphorylated extracellular signal-regulated kinase (ERK)-1/2, Bcl-xL, Bad, Bax, and cleaved caspase 3 antibodies (New England BioLabs, Beverly, Massachusetts); SOCS3 (Immuno-Biological Laboratories, Takasaki, Japan); cytochrome c (BD Pharmingen, Franklin Lakes, New Jersey); porin (Invitrogen, Carlsbad, California); tubulin (Santa Cruz Biotechnology, Santa Cruz, California); mitochondrial transcriptional factor A (TFAM) (26); manganese superoxide dismutase (Mn-SOD); and heme oxygenase (HO)-1 (Abcam, Cambridge, United Kingdom).

TUNEL staining. To detect apoptosis, terminal deoxynucleotidyl transferase-mediated dUTP nick end-labeling (TUNEL) staining was performed according to the manufacturer's protocol (In Situ Apoptosis Detection kit; Takara

Abbreviations and Acronyms

AMI = acute myocardial infarction
CKO = cardiac-specific knockout mice
ERK = extracellular signal-regulated kinase
flox = flanked byloxP site
G-CSF = granulocyte colony-stimulating factor
HO = heme oxygenase
IL = interleukin
JAK = janus kinase
LIF = leukemia inhibitory factor
LPS = lipopolysaccharide
LV = left ventricular
Mn-SOD = manganese superoxide dismutase
PCR = polymerase chain reaction
PGC = peroxisome proliferator-activated receptor-gamma coactivator
ROS = reactive oxygen species
RNA = ribonucleic acid
SOCS = suppressor of cytokine signaling
STAT = signal transducer and activator of transcription
TFAM = mitochondrial transcriptional factor A
TTC = triphenyltetrazolium chloride
TUNEL = terminal deoxynucleotidyl transferase-mediated dUTP nick end-labeling

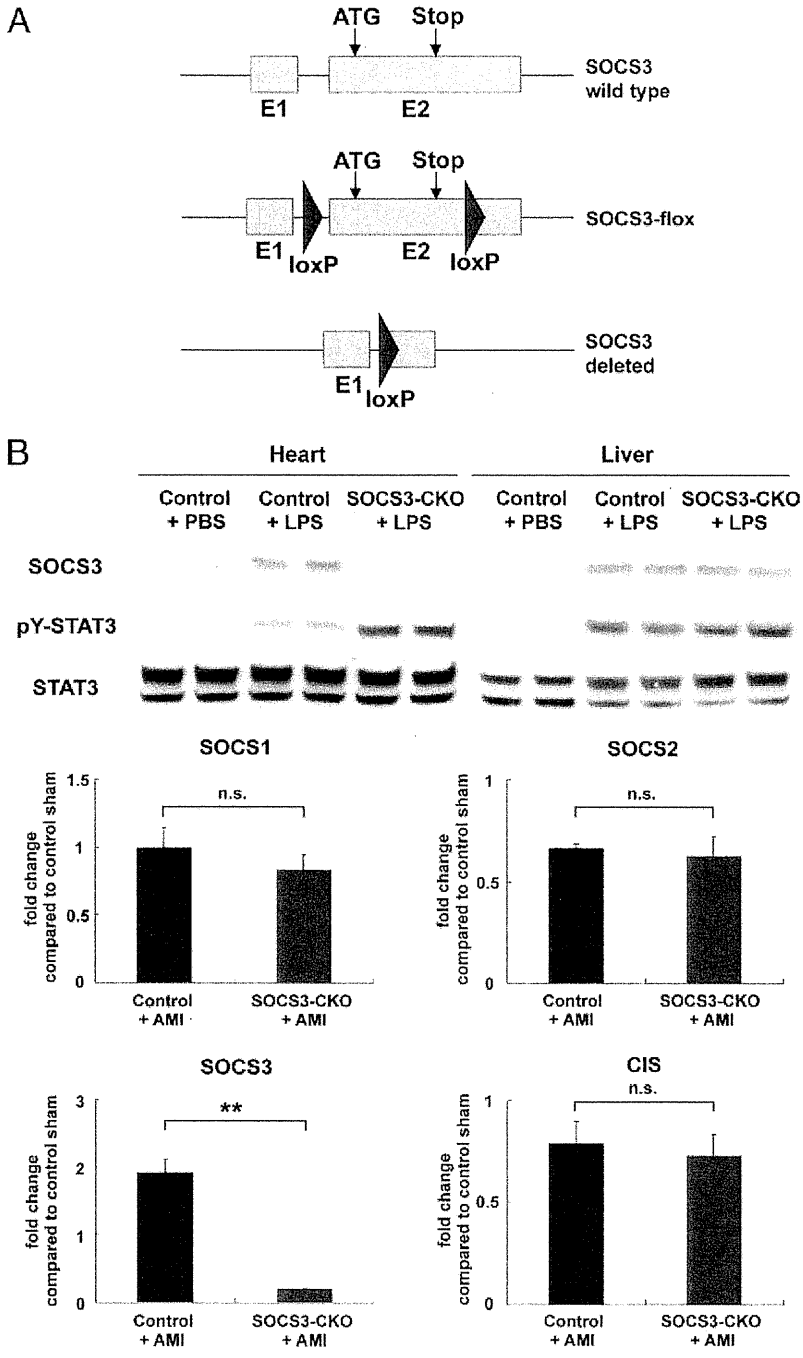

Figure 1 Generation of Cardiac-Specific SOCS3 Knockout Mice

(A) The wild-type suppressor of cytokine signaling-3 (SOCS3) allele was modified by inserting loxP sites flanking the coding lesion in the second exon2 (E2) of SOCS3. The first exon (E1) and E2 are shown as boxes, and the SOCS3 coding region is indicated by the ATG and stop codons. Wild-type SOCS3, the targeted SOCS3 locus (SOCS3-flox), and the deleted locus (SOCS3-deleted) are shown. **(B)** SOCS3, phospho-STAT3 (pY-STAT3), and STAT3 expression in heart and liver after lipopolysaccharide (LPS) injection were examined using Western blot analysis with SOCS3, phospho-STAT3, and STAT3 antibodies, respectively. **(C)** Real-time PCR analyses for expression of SOCS family genes, including SOCS3, SOCS1, SOCS2, and cytokine-inducible SH2 protein (CIS) in the hearts after acute myocardial infarction (AMI). PBS = phosphate-buffered saline; n.s. = not statistically significant. $^{**}p < 0.01$.

Bio Inc., Otsu, Japan). Digital photographs were taken at 400× magnification, and 25 random high-power fields from each heart sample were chosen and quantified.

RNA extraction and real-time PCR. Total LV ribonucleic acid (RNA) was isolated using TRIzol (Invitrogen) as described previously (20–22), and 1 μg of total RNA was converted into complimentary deoxyribonucleic acid. Expression profiles of common cytokines were performed with the RT2 Profiler polymerase chain reaction (PCR) array for murine common cytokines (SABiosciences, Frederick, Maryland), according to the manufacturer's instructions. Polymerase chain reaction was performed with the StepOne real-time PCR machine (Applied Biosystems, Foster City, California). The $\Delta\Delta C_t$ method was used to analyze the expression level of each gene. After PCR, the dissociation curve for each gene was examined to exclude genes with nonspecific amplification or undetectable expression. The expression profile of each gene was displayed as a heat map made by using MeV MultiExperiment Viewer 4.1 (Institute for Genomic Research, Rockville, Maryland). Real-time PCR assays were also performed to assess the gene expression of mouse SOCS1, SOCS2, SOCS3, cytokine-inducible SH2 protein (CIS), peroxisome proliferator-activated receptor-gamma coactivator 1-alpha (PGC-1α), collagen 1, and collagen 32, and GADPH with the corresponding primer pairs (Applied Biosystems, #Mm00782550_s1 refer to SOCS1, #Mm00850544 g1 refer to SOCS2, #Mm00545913 s1 refer to SOCS3, #Mm01230623_g1 refer to CIS, #Mm01208835_m1 refer to PGC-1α, Mm01254476_ml refer to collagen 3, and #Mm99999915_g1 refer to GADPH, respectively) using the StepOnePlus Real-Time PCR System (Applied Biosystems).

Echocardiogram. At 14 days after AMI, transthoracic echocardiographic studies were performed under light anesthesia using a Vevo770 ultrasound machine (VisualSonics Inc., Toronto, Ontario, Canada) equipped with a 30-MHz probe. Mice were anesthetized with isoflurane and subjected to echocardiography as previously described (20–22). Recording was performed as described previously (20–22).

Statistical analysis. Data are expressed as mean ± standard error (SE). Multiple group comparisons were performed using 1-way analysis of variance followed by the Bonferroni procedure for comparison of means (Figs. 2C, 3B, 4B, 6A, 7A, and 9A). Comparison of 2 groups was analyzed using 2-tailed Student's *t* test. Survival analysis was performed using the Kaplan-Meier method, and between-group differences in survival were tested using the log-rank (Mantel-Cox) test; p values <0.05 were considered statistically significant.

Results

Basal phenotype of SOCS3-CKO. SOCS3-CKO pups were born in an expected Mendelian ratio and grew to adulthood normally. We confirmed by Western blot that SOCS3 expression was induced in LPS-injected hearts of control mice. SOCS3 expression was markedly reduced in LPS-injected SOCS3-CKO hearts, and was accompanied by enhanced STAT3 phosphorylation (Fig. 1B). We also confirmed using real-time PCR that SOCS3 messenger RNA was markedly reduced in SOCS3-CKO hearts 2 days after AMI, and that the expression of other SOCS family genes including SOCS1 were not altered in controls or SOCS3-CKO hearts (Fig. 1C). Histological examination of SOCS3-CKO hearts at 16 weeks revealed no evidence of necrosis or ventricular fibrosis. Echocardiography confirmed preserved LV function and wall thickness in SOCS3-CKO, comparable to littermate controls (data not shown).

Prevention of post-infarct LV remodeling and mortality in SOCS3-CKO. We first evaluated the initial infarct size 3 h after coronary ligation using Evans blue dye and TTC staining. Both the area at risk and infarct size immediately after AMI were comparable between controls and SOCS3-CKO (Fig. 2A). We then compared the survival rate between controls and SOCS3-CKO. Approximately 45% of controls died within 14 days after AMI (Fig. 2B). In contrast, all SOCS3-CKO survived up to 14 days after AMI. The increases in LV weight-to-body-weight ratio and lung weight-to-body-weight ratio 14 days after AMI were significantly attenuated in SOCS3-CKO compared with controls (Fig. 2C). Mallory-AZAN staining revealed that the infarct area of hearts 14 days after AMI was significantly smaller in SOCS3-CKO than in controls (Fig. 2D). Echocardiographic assessment consistently revealed that anterior wall thickness was greater, LV end-diastolic dimension was smaller, and ejection fraction was greater in SOCS3-CKO than in controls 14 days after AMI (Fig. 3). Thus, post-infarct LV remodeling and mortality were significantly prevented in SOCS3-CKO.

Enhanced activation of cardioprotective signaling pathways in SOCS3-CKO after AMI. Next, we compared the activation of cardioprotective signaling pathways including STAT3, STAT1, AKT, and ERK1/2 after AMI in controls and SOCS3-CKO using Western blot analysis. Whereas STAT3 and STAT1 were promptly phosphorylated and AKT was phosphorylated 3 days after AMI, ERK1/2 phosphorylation was down-regulated up to 7 days after AMI in controls (Fig. 4A). Consistent with a previous report that cytokine-induced SOCS3 expression is STAT3-dependent, SOCS3 induction was closely correlated with STAT3 activation in the hearts of controls. In SOCS3-CKO hearts compared with controls, STAT3 phosphorylation was greater and more sustained, STAT1 phosphorylation was less, and phosphorylation of AKT and ERK1/2 was more rapid and greater up to 14 days after AMI (Fig. 4A). Thus, the activation of cardioprotective signaling pathways including STAT3, AKT, and ERK1/2 after AMI was enhanced in SOCS3-CKO compared with controls. We also conducted immunohistochemical staining of phosphorylated STAT3 in the heart after AMI. The number of phosphorylated STAT3 positive cells was significantly greater in SOCS3-CKO hearts than that in control hearts in both the border area and the remote area (Fig. 4B).

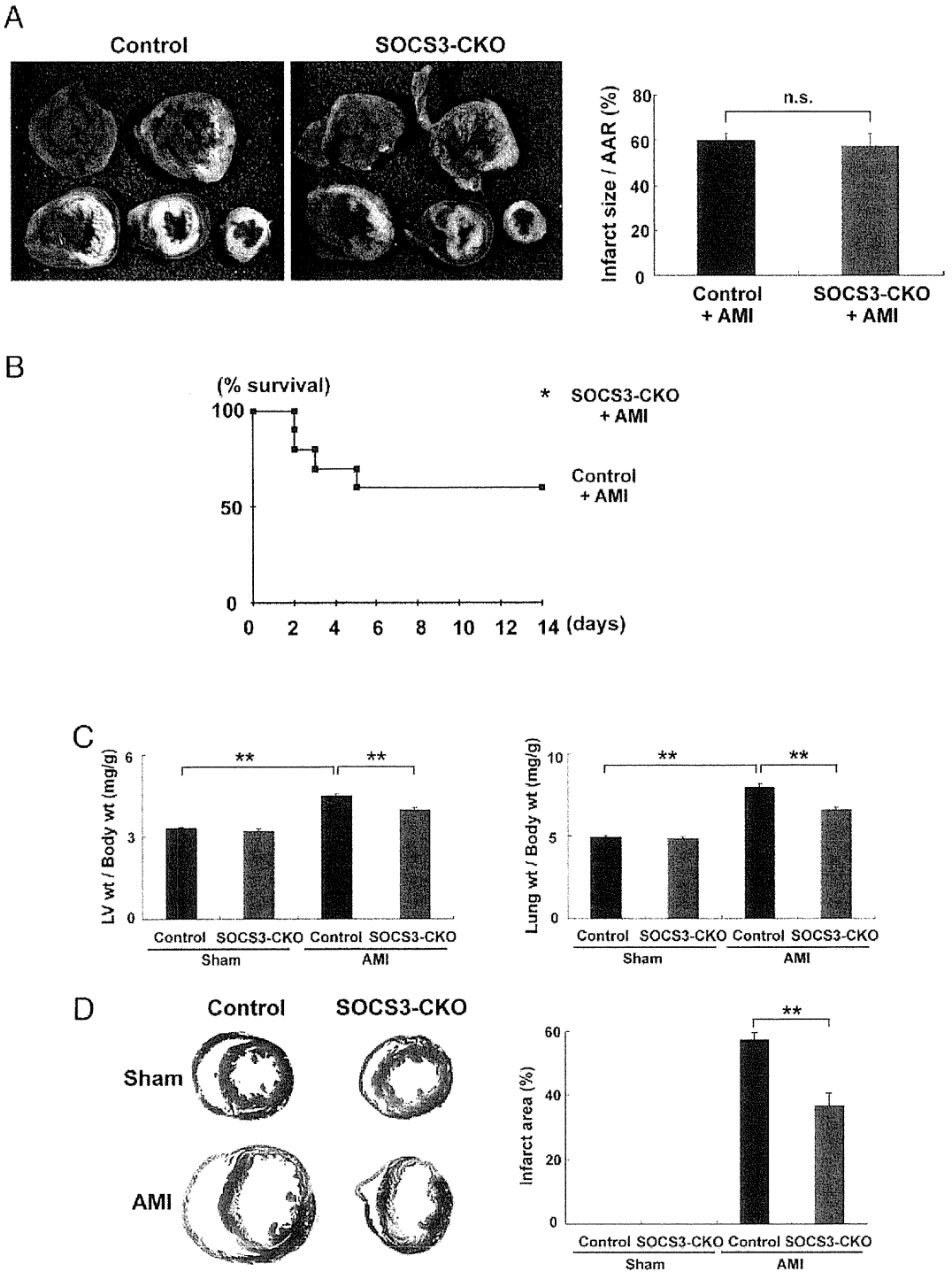

Figure 2 Decreased LV Remodeling and Mortality After AMI in SOCS3-CKO

(A) Evans blue dye and triphenyltetrazolium chloride staining of control **(left)** and cardiac-specific suppressor of cytokine signaling-3 knockout mice (SOCS3-CKO) **(center)** hearts 3 h after acute myocardial infarction (AMI) (n = 5). Left ventricular (LV) infarct size was expressed as percentage of the area at risk (AAR) in each group **(right)**. **(B)** Kaplan-Meier survival analysis of controls and SOCS3-CKO after AMI (n = 10 mice for each group; *$p < 0.05$ vs. controls). **(C)** LV to body weight ratio **(left)** and lung to body weight ratio **(right)** in controls and SOCS3-CKO 14 days after AMI (n = 6 to 10). **$p < 0.01$ (Bonferroni adjusted; 2 comparisons). **(D)** Mallory-AZAN staining of sham and AMI in control and SOCS3-CKO hearts 14 days after AMI (n = 6 to 10). ** $p < 0.01$ versus controls 14 days after AMI.

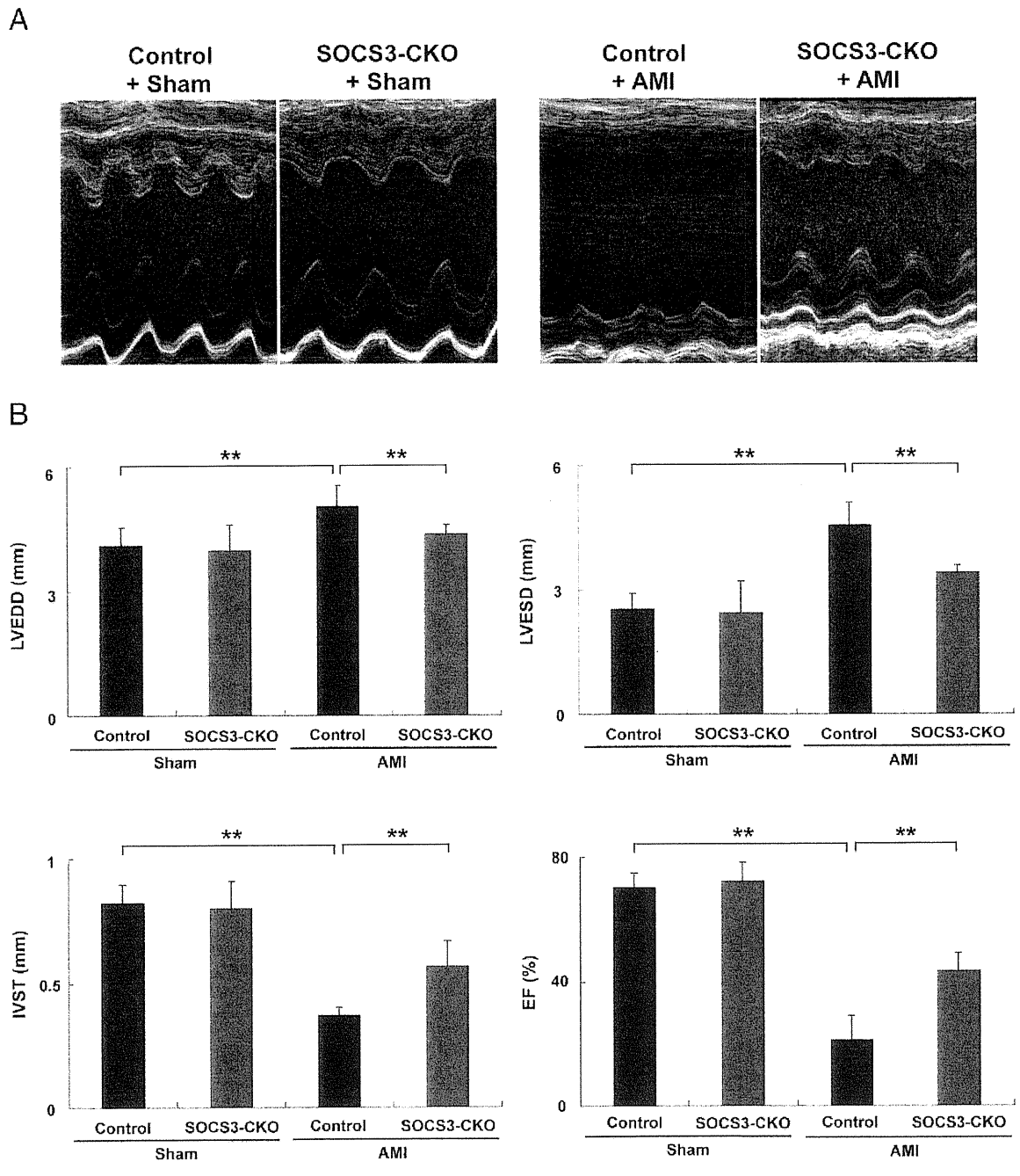

Figure 3 Prevention of LV Dilation and Dysfunction in SOCS3-CKO After AMI

Echocardiography was performed 14 days after sham operation or acute myocardial infarction (AMI) (n = 10 mice for each group). **(A)** Representative M-mode echocardiograms obtained from 4 groups. **(B)** Pooled data for echocardiographic measurements in 4 groups of mice. **p < 0.01 (Bonferroni adjusted; 2 comparisons). IVST = intraventricular septal thickness; LVEDD = left ventricular end-diastolic diameter; other abbreviations as in Figure 2.

Cytokine-rich microenvironment in the heart after AMI. To determine which cytokine activates JAK downstream signaling pathways in the heart after AMI, we conducted real-time PCR analysis for cytokines on mice hearts 2 days after AMI. Multiple cytokines that activate the JAK-STAT pathway and induce SOCS3 expression were highly expressed in the heart after AMI, demonstrating the presence of a cytokine-rich microenvironment in the ischemic myo-

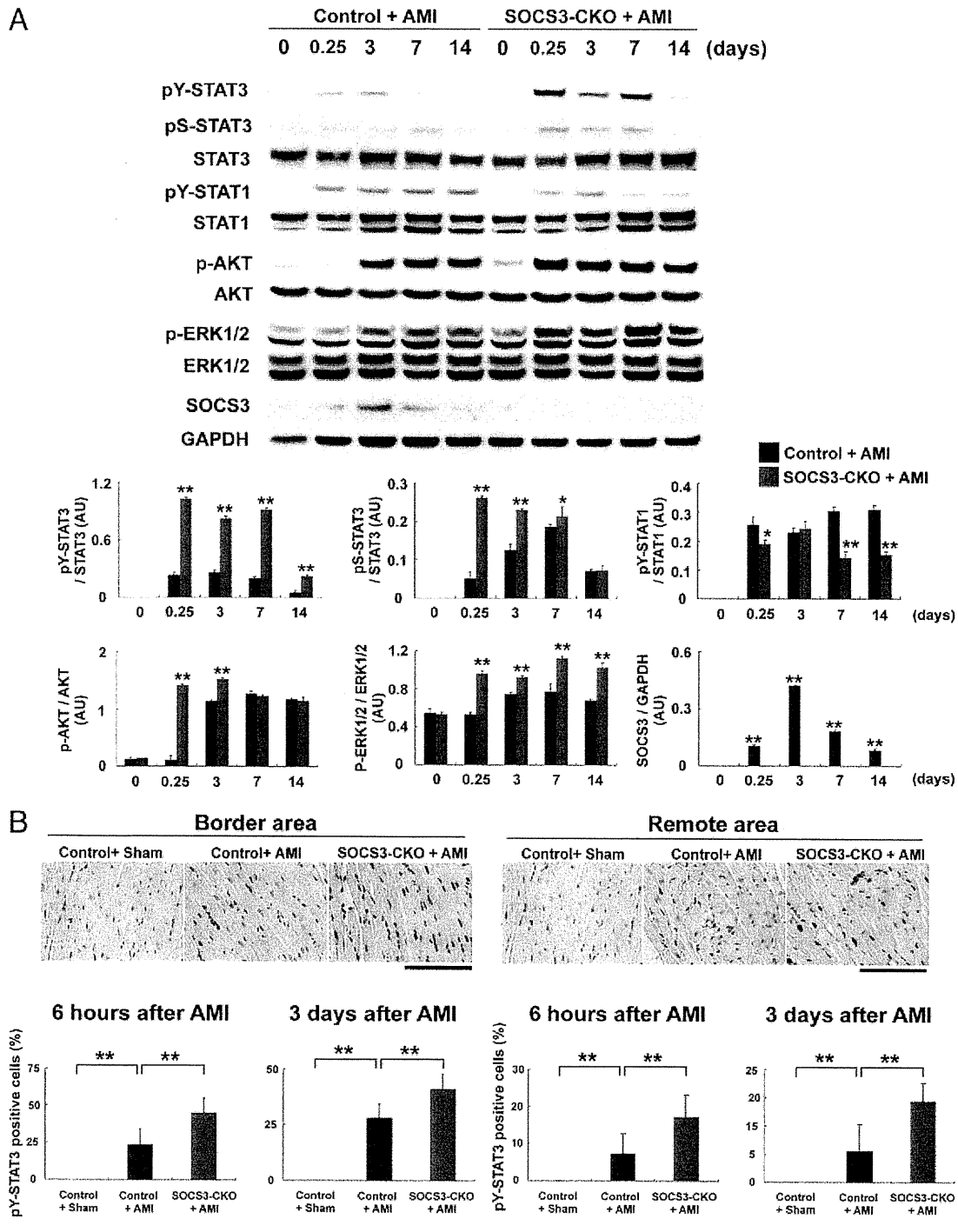

Figure 4 **Enhanced Activation of Cardioprotective Signaling Pathways in SOCS3-CKO Hearts After AMI**

(A) Total cell lysate was prepared from the left ventricle of controls or SOCS3-CKO at the indicated times after AMI, and blotted with antibodies raised against tyrosine-phosphorylated STAT3 (pY-STAT3), serine-phosphorylated STAT3 (pS-STAT3), phosphorylated AKT (p-AKT), phosphorylated ERK1/2 (p-ERK1/2), SOCS3, and glyceraldehyde 3-phosphate dehydrogenase (GAPDH). Bar graphs represent quantitative differences in pY-STAT3, pS-STAT3, p-AKT, p-ERK1/2, and SOCS3 expression (n = 5 for each). **p < 0.01 versus controls after AMI; *p < 0.05 versus controls after AMI. **(B)** Immunostaining of pY-STAT3 in hearts after sham operation or AMI (n = 10 for each). Representative photographs of the border and remote areas in hearts from each group. Values are expressed as the percentage of pY-STAT3 positive cells in the hearts 6 h or 3 days after AMI. **p < 0.01 (Bonferroni adjusted; 2 comparisons). Scale bar = 100 μm. AU = arbitrary units; other abbreviations as in Figure 2.

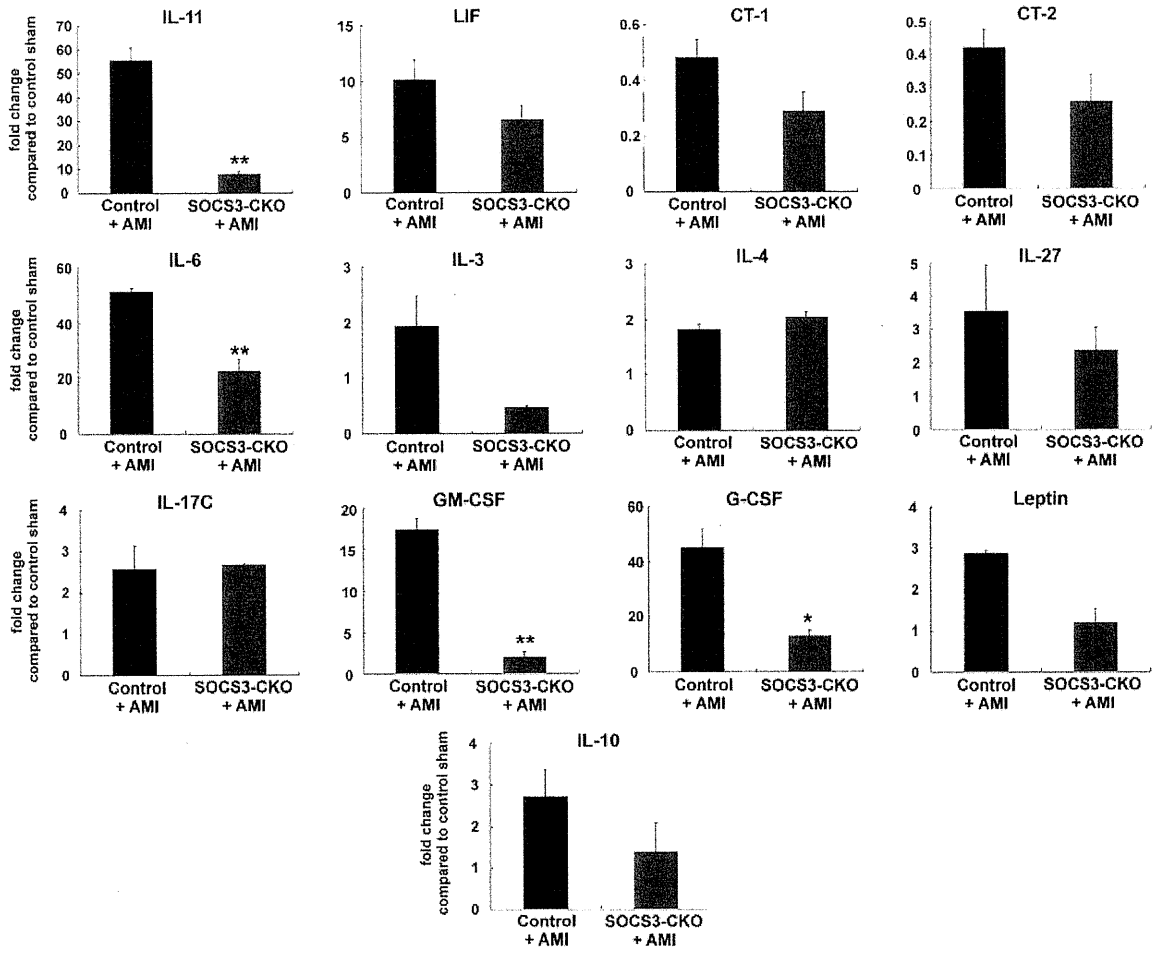

Figure 5 Expression of JAK-STAT–Activating Cytokines in Control and SOCS3-CKO Hearts After AMI

Messenger ribonucleic acid was prepared from the left ventricle of control mice or SOCS3-CKO 2 days after AMI and real-time polymerase chain reaction (PCR) analyses for cytokines were performed. Values normalized to glyceraldehyde 3-phosphate dehydrogenase are expressed as fold change from the values of sham mice (n = 5 for each group). **p < 0.01 versus controls. *p < 0.05 versus controls. CT = cardiotrophin; G-CSF = granulocyte colony-stimulating factor; GM-CSF = granulocyte-macrophage colony-stimulating factor; IL = interleukin; JAK = *janus* kinase; STAT = signal transducer and activator of transcription; other abbreviations as in Figure 2.

cardium (Fig. 5). Expressions of several cytokines including G-CSF and IL-11 were lower in SOCS3-CKO hearts than that in controls (Fig. 5).

Inhibition of cardiomyocyte apoptosis in SOCS3-CKO after AMI. To determine the mechanism underlying how SOCS3 deletion in cardiomyocytes prevents the development of LV remodeling, we first measured the number of apoptotic cells by TUNEL staining 24 h after AMI. The number of TUNEL-positive cells was significantly smaller in SOCS3-CKO hearts than in controls (Fig. 6A). Western blot analysis revealed that expression of the antiapoptotic molecule Bcl-xL was much greater in SOCS3-CKO than in controls. On the other hand, the expression of proapoptotic molecules Bad and Bax was less in SOCS3-CKO than in controls (Fig. 6B). The release of cytochrome c into the cytosol after AMI was also smaller in SOCS3-CKO hearts than in controls (Fig. 7A).

Increased PGC-1α and TFAM expressions in SOCS3-CKO hearts after AMI. Because PGC-1α and TFAM play important roles in cardiac mitochondrial biology (26–28), we examined PGC-1α and TFAM expressions in infarct hearts using real-time PCR and Western blot analysis, respectively. We observed that PGC-1α expression after AMI was greater in SOCS3-CKO hearts than in controls (Fig. 7B). We observed that TFAM expression was much greater in SOCS3-CKO hearts than in controls (Fig. 7C). Additionally, we conducted immunohistochemical staining of TFAM in the heart after AMI. The number of TFAM-positive cells was significantly greater in SOCS3-CKO hearts than in controls, both in the border area and in the remote area (Fig. 7D).

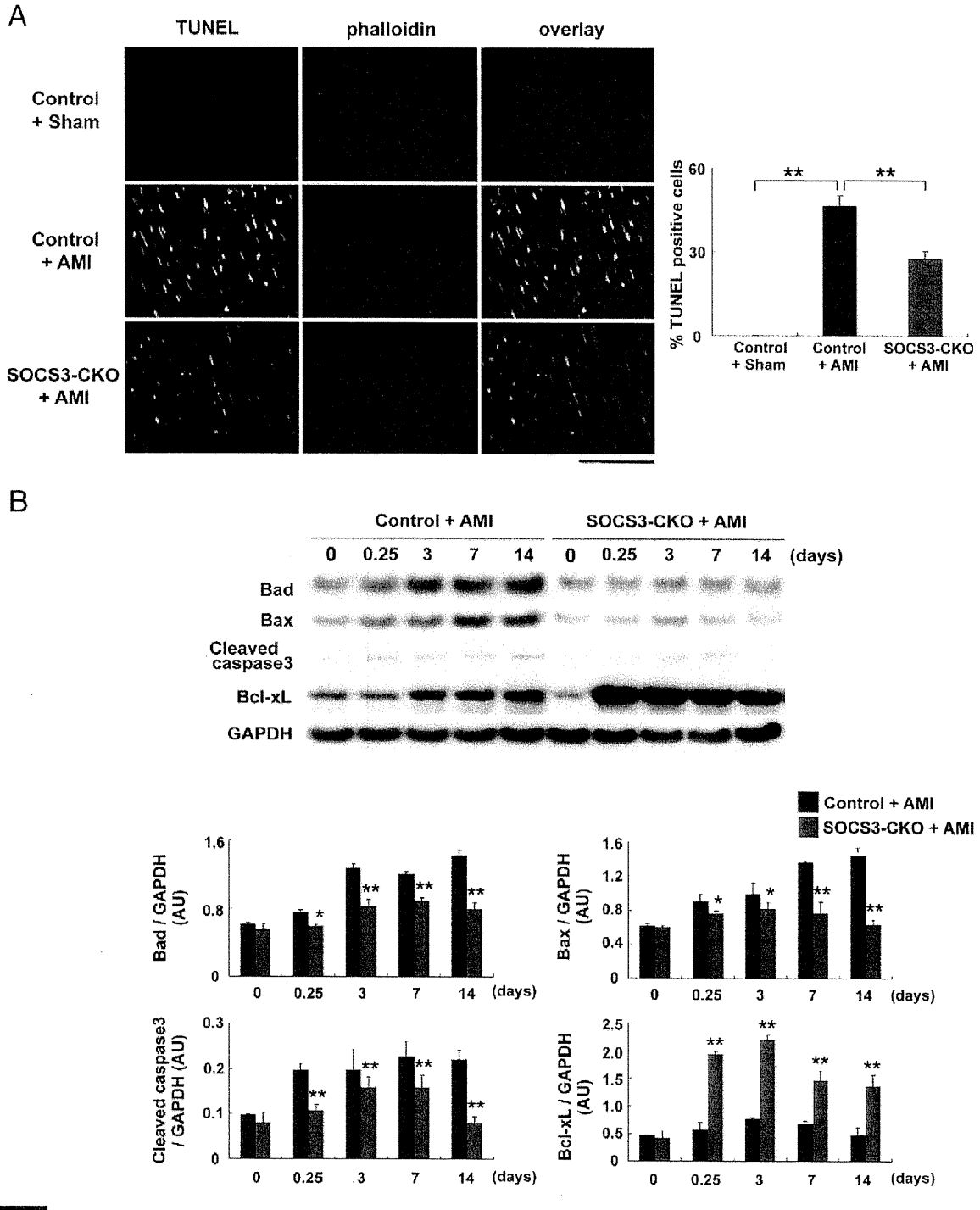

Figure 6 Inhibition of Apoptosis in SOCS3-CKO Hearts After AMI

(A) Terminal deoxynucleotidyl transferase-mediated dUTP nick end-labeling (TUNEL) staining control or SOCS3-CKO hearts 24 h after sham operation or AMI (n = 5 for each group). Representative photographs of border area in hearts from each group **(left)**. The graph shows the percentage of TUNEL-positive cells **(right)**. **p < 0.01 (Bonferroni adjusted; 2 comparisons). Scale bar = 100 μm. **(B)** Total cell lysate was prepared from the left ventricle of controls or SOCS3-CKO at the indicated times after AMI, and blotted with antibodies raised against Bcl-xL, Bad, Bax, and cleaved caspase 3. Bar graphs represent the quantitative differences in Bcl-xL, Bad, Bax, and cleaved caspase 3 expression (n = 5 for each). **p < 0.01 versus controls after AMI. *p < 0.05 versus controls after AMI. AU = arbitrary units; GAPDH = glyceraldehyde 3-phosphate dehydrogenase; other abbreviations as in Figure 2.

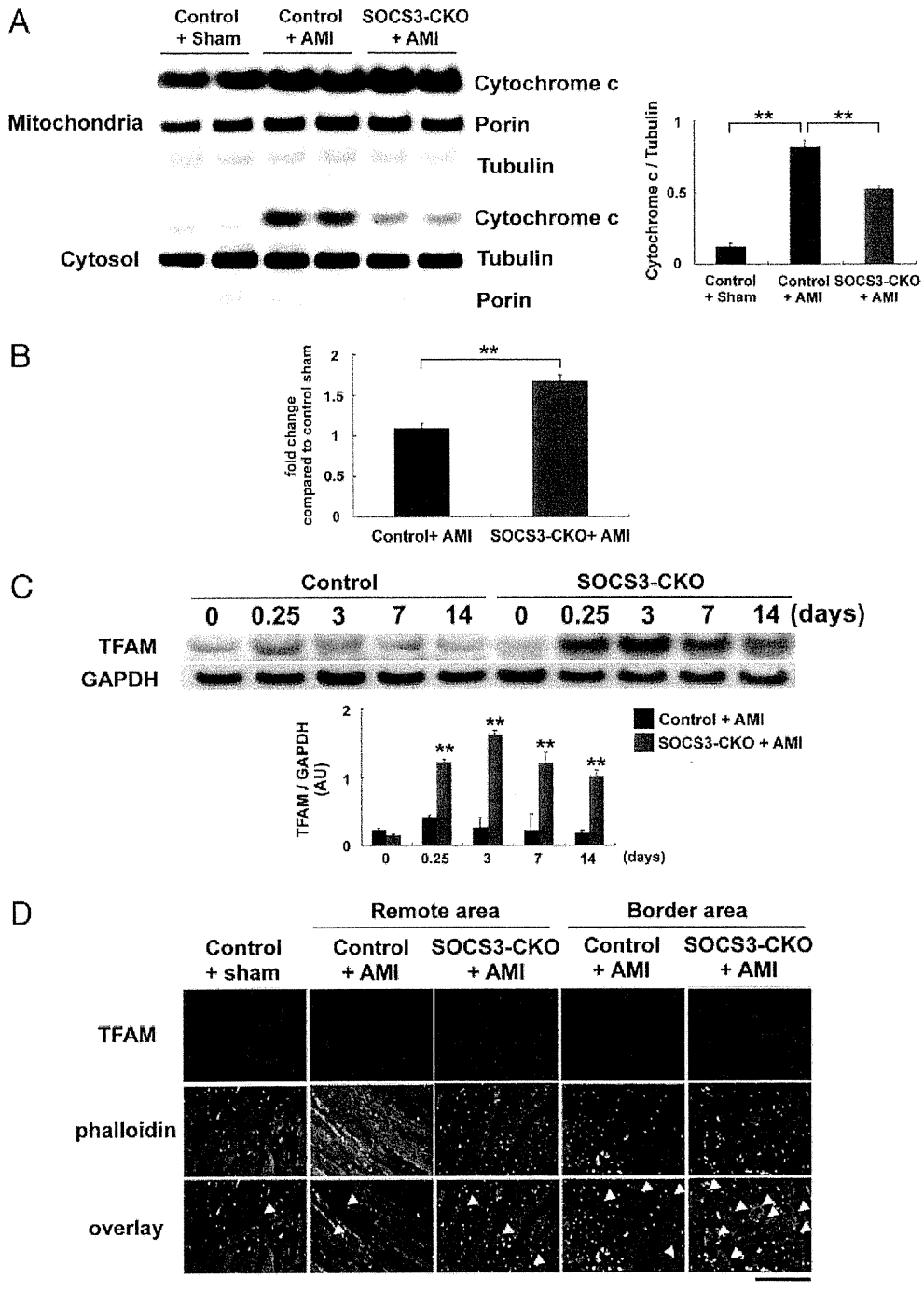

Figure 7 Increased PGC-1α and TFAM Expression in SOCS3-CKO Hearts After AMI

(A) The cytosolic and mitochondrial fractions were prepared from the left ventricles (LV) of controls or SOCS3-CKO 6 h after AMI and blotted with anticytochrome c antibody. Porin and tubulin expression were examined as internal controls (n = 5 for each). The experiments were repeated three times, yielding similar results. **p < 0.01 (Bonferroni adjusted; 2 comparisons). **(B)** Messenger ribonucleic acid was prepared from the LV of controls or SOCS3-CKO 2 days after AMI, and real-time polymerase chain reaction (PCR) analysis for peroxisome proliferator-activated receptor-gamma coactivator 1-alpha (PGC-1α) was performed. Values normalized to glyceraldehyde 3-phosphate dehydrogenase (GAPDH) are expressed as fold change from the values of sham mice (n = 5 for each group). **p < 0.01 versus controls; *p < 0.05 versus controls. **(C)** Total cell lysate was prepared from the LV of controls or SOCS3-CKO at the indicated times after AMI, and blotted with anti-mitochondrial transcriptional factor A (TFAM) antibody. Bar graphs represent quantitative differences in TFAM expression (n = 5 for each). **p < 0.01 versus controls after AMI. **(D)** Induction of TFAM expression in the viable border area and remote area. LV sections were costained with anti-TFAM antibody **(red)** and phalloidin **(green)** 3 days after AMI. Scale bar = 100 μm. AU = arbitrary units; other abbreviations as in Figure 2.

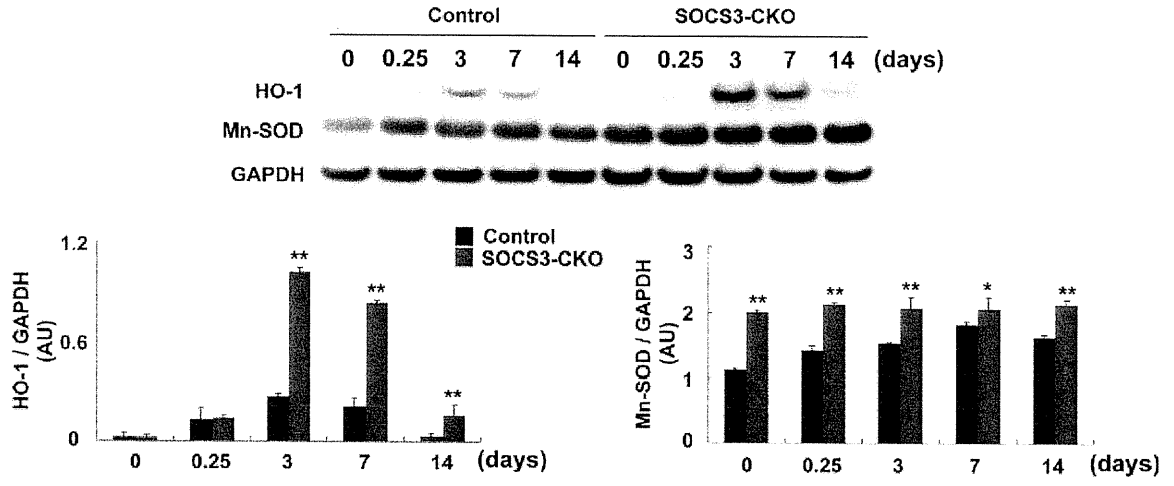

Figure 8 Increased Expression of Antioxidant Molecules in SOCS3-CKO Hearts After AMI

Western blot analyses for heme oxygenase-1 (HO-1) and manganese superoxide dismutase (MnSOD) were performed (n = 5 for each group). Total cell lysate was prepared from left ventricles of controls or SOCS3-CKO at the indicated times after AMI, and blotted with anti–HO-1 and anti-MnSOD antibodies. Bar graphs represent quantitative differences in HO-1 and MnSOD expression (n = 5 for each). **$p < 0.01$ versus controls after AMI; *$p < 0.05$ versus controls after AMI. AU = arbitrary units; other abbreviations as in Figure 2.

Enhancement of antioxidant enzymes expression in SOCS3-CKO hearts after AMI. It is well known that mitochondria are major sources of reactive oxygen species (ROS) and that ROS themselves promote mitochondria-mediated myocardial apoptosis (28,29). Antioxidants such as Mn-SOD and HO-1 prevent LV remodeling after AMI (30,31). Western blot analysis revealed that expressions of HO-1 and Mn-SOD were significantly greater in SOCS3-CKO hearts after AMI (Fig. 8).

Decreased cardiac fibrosis in SOCS3-CKO hearts after AMI. Cardiac fibrosis is a critical feature of post-infarct LV remodeling. Therefore, we measured the fibrotic area in Mallory-AZAN–stained hearts 14 days after AMI, and conducted real-time PCR for genes that were involved in fibrosis and related to the JAK-STAT pathway. The fibrotic areas were smaller in SOCS3-CKO hearts than in controls in both infarct and remote areas (Fig. 9A). Expression of matrix metalloproteinase-9, connective tissue growth factor, transforming growth factor β2, collagen 1, and collagen 3 was significantly lower and expression of tissue inhibitor of matrix metalloproteinase-2 was significantly greater in SOCS3-CKO than in controls (Fig. 9B).

Discussion

In the present study, we attempted to determine the role of SOCS3, which is an intrinsic negative regulator of multiple cytokines, within cardiomyocytes in the development of LV remodeling after AMI. We observed that the deletion of SOCS3 in cardiomyocytes enhanced multiple survival pathways including STAT3, AKT, and ERK1/2; prevented myocardial apoptosis and fibrosis; enhanced the expression of antioxidants; and resulted in the prevention of LV remodeling after AMI. Our findings suggest that cardiac SOCS3 may be a key molecule for the development of LV remodeling after AMI.

We consider that the enhanced survival of SOCS3-CKO after AMI is due to the inhibitions of LV remodeling and the subsequent heart failure. It is possible that the inhibitions of LV remodeling and heart failure after AMI in SOCS3-CKO are due to the decreased infarct size. However, the initial infarct size 3 h after coronary occlusion was similar between SOCS3-CKO and controls. On the other hand, the infarct size 14 days after AMI was significantly smaller in SOCS3-CKO than in controls, indicating that progression of LV remodeling after AMI was inhibited in SOCS3-CKO hearts. On the basis of these results, we will discuss the cardioprotective mechanisms against LV remodeling after AMI in mice with a cardiac-specific SOCS3 deletion.

In our previous study, forced expression of SOCS3 in ventricular cardiomyocytes completely suppressed the anti-apoptotic action of cardiotrophin-1 and LIF by inhibiting STAT3, AKT, and ERK1/2 signaling pathways (20), suggesting that cardiac SOCS3 may promote apoptosis under pathological conditions in which JAK-STAT signaling pathways are activated. Consistent with the previous study, Harada et al. (5) recently demonstrated that the cardiac-specific inhibition of STAT3 by the transgenic expression of dominant-negative STAT3 abolished the beneficial effects of G-CSF on LV remodeling after AMI. They proposed that the direct action of G-CSF on cardiomyocytes via the JAK-STAT3 signaling pathway plays a crucial role in

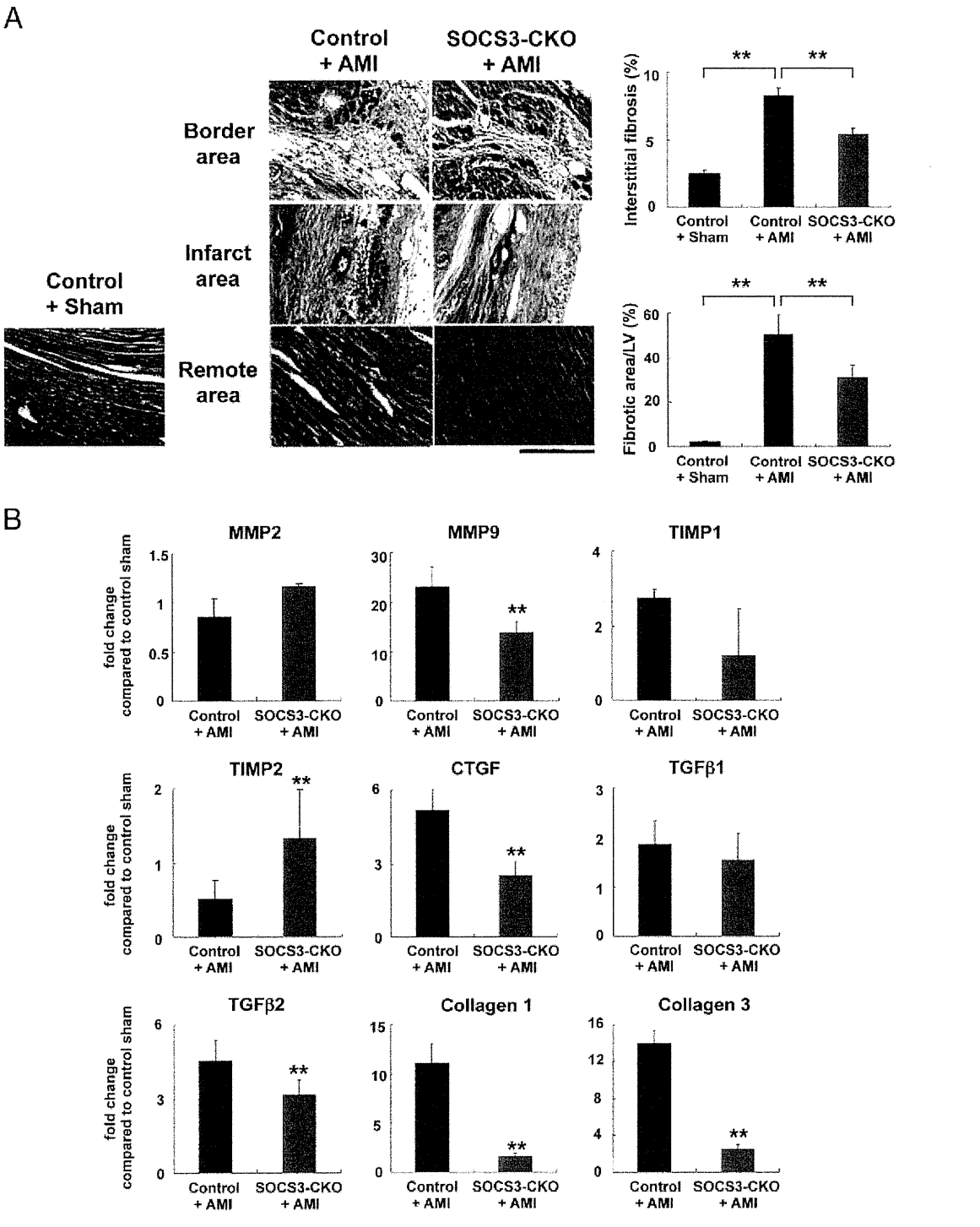

Figure 9 Decreased Cardiac Fibrosis in SOCS3-CKO Hearts After AMI

(A) Mallory-AZAN staining of myocardial sections 14 days after AMI. Less fibrotic area was observed in SOCS3-CKO hearts than in controls. Quantitative analysis revealed significantly less fibrotic area in both infarct and remote areas. **$p < 0.01$ (Bonferroni adjusted; 2 comparisons). **(B)** Messenger ribonucleic acid was prepared from the LV of controls or SOCS3-CKO after AMI, and real-time polymerase chain reaction analyses for indicated genes were performed. Values normalized to glyceraldehyde 3-phosphate dehydrogenase are expressed as fold change from the values of sham mice ($n = 5$ for each group). **$p < 0.01$ versus controls: *$p < 0.05$ versus controls. CTGF = connective tissue growth factor; MMP = matrix metalloproteinase; TGF = transforming growth factor; TIMP = tissue inhibitor of metalloproteinase; other abbreviations as in Figure 2.

JACC Vol. 59, No. 9, 2012
February 28, 2012:838–52

preventing myocardial apoptosis after AMI (5). In the present study, SOCS3 was not induced within a few hours after coronary occlusion but was induced several hours after coronary occlusion in control mice. We demonstrated that the cardiac-specific deletion of SOCS3 prevented myocardial apoptosis and LV remodeling after AMI by augmenting STAT3 activation. Although the initial infarct size was comparable between SOCS3-CKO and controls, the number of apoptotic cells 24 h after coronary occlusion was significantly less in SOCS3-CKO than in controls, suggesting that myocardial apoptosis during infarct expansion after AMI was prevented in SOCS3-CKO hearts. Taken together, our results suggest that ischemia-induced SOCS3 induction in cardiomyocytes may facilitate myocardial apoptosis in infarct expansion during LV remodeling after AMI.

Next we investigated the mechanisms underpinning attenuated apoptosis in SOCS3-CKO hearts. We focused on mitochondria of cardiomyocytes for 2 reasons. First, it has been shown that mitochondria play an important role in the regulation of apoptosis. Second, it is well known that the antiapoptotic protein Bcl-xL is a STAT3 target gene, which governs mitochondrial outer membrane permeabilization and suppresses apoptosis (32,33). Recently, Wegrzyn et al. (34) demonstrated a novel function of serine-phosphorylated STAT3 in mitochondrial homeostasis. They reported that serine-phosphorylated STAT3 was present in the mitochondria of primary tissues including the heart, and that the activities of complexes I and II of the electron transport chain were significantly decreased in STAT3-deficient cells (34). In the present study, we have several lines of evidence for preserved mitochondrial function in SOCS3-CKO hearts. We have shown that the release of cytochrome c from mitochondria to the cytosol was prevented in the heart of SOCS3-CKO after AMI (Fig. 7). Both tyrosine-phosphorylated STAT3 and serine-phosphorylated STAT3 were significantly enhanced in SOCS3-CKO hearts (Fig. 4A). We also observed that TFAM (an essential molecule for the mitochondrial deoxyribonucleic acid transcription and replication) (26,35) and PGC-1α (an important regulator of mitochondrial biology in the heart) (27) were transiently up-regulated after AMI, and their expression was enhanced in SOCS3-CKO hearts. Taken together, the present study may indicate that cardiac-specific deletion of SOCS3 enhances STAT3 activation and prevents mitochondria-mediated myocardial apoptosis.

Next we investigated the mechanism underpinning the prevention of mitochondria-mediated myocardial apoptosis in SOCS3-CKO hearts. In addition to the role of mitochondria as a source of ROS, mitochondria themselves are damaged by ROS (28,29). ROS induce myocardial apoptosis, which plays an important role in the development and progression of maladaptive LV remodeling after AMI (28,29). Antioxidant enzymes such as Mn-SOD and HO-1 are defense mechanisms against ROS-mediated myocardial injury. It has been shown that both Mn-SOD and HO-1 prevent myocardial apoptosis and LV remodeling after AMI (30,31). Mn-SOD and HO-1 are target genes of STAT3 (36,37). In the present study, we found that HO-1 expression was transiently and Mn-SOD was gradually up-regulated after AMI in hearts from controls (Fig. 8). Additionally, Mn-SOD and HO-1 expression are enhanced during LV remodeling after AMI in SOCS3-CKO hearts. Therefore, increased Mn-SOD and HO-1 expression may have contributed to the prevention of mitochondria-mediated myocardial apoptosis, leading to the inhibition of LV remodeling after AMI in SOCS3-CKO (Fig. 10).

Cardiac fibrosis is a critical feature of post-infarct LV remodeling. STAT3-activating cytokines such as IL-11, G-CSF, and erythropoietin suppress cardiac fibrosis during AMI (10,38,39). Cardiac-specific STAT3-deficient mice exhibited a marked increase of cardiac fibrosis (40). In this study, we found that cardiac fibrosis in SOCS3-CKO was reduced compared with controls, and that the expressions of connective tissue growth factor, matrix metalloproteinase-9, and transforming growth factor β2, which promote cardiac fibrosis, was reduced in SOCS3-CKO hearts compared with controls. These results suggest that preventions of myocardial apoptosis as well as fibrosis may contribute to the inhibition of post-infarct LV remodeling in SOCS3-CKO.

In this study, the enhancement of STAT3 activation and TFAM expression, and the reduction of fibrotic response, were observed in both infarct and remote viable areas during LV remodeling after AMI. These results suggest an important underlying mechanism by which the myocardium of SOCS3-CKO was protected from either ischemic injury directly or post-AMI stress throughout the myocardium.

Because we demonstrated that myocardial-specific SOCS3 deletion enhanced multiple cardioprotective signaling pathways and ameliorated LV remodeling after AMI, small-molecule antagonist of SOCS3 or tissue-specific vector delivery of SOCS3 inhibitor during LV remodeling after AMI may prove to be a clinically valuable strategy to enhance the protective effect of JAK-STAT–activating cytokines. Recently, the first phase II trial showed that an intravenous bolus of erythropoietin did not reduce infarct size in patients with AMI (41). We previously showed that cytokine-induced SOCS3 confers resistance to cytokine action by inhibiting the JAK-STAT pathway (42,43). Therefore, the strategy of myocardial SOCS3 inhibition may be effective for AMI patients who are resistant to cytokines such as erythropoietin.

We propose that myocardial SOCS3 is a key determinant of LV remodeling after AMI, and SOCS3 may serve as a novel therapeutic target to prevent LV remodeling after AMI. Cardiac-specific STAT3-deficient mice exhibited a maladaptive cardiac remodeling with aging (40). Therefore, although the experiments reported here were restricted to young mice, the long-term effects of SOCS3 deletion remain to be determined.

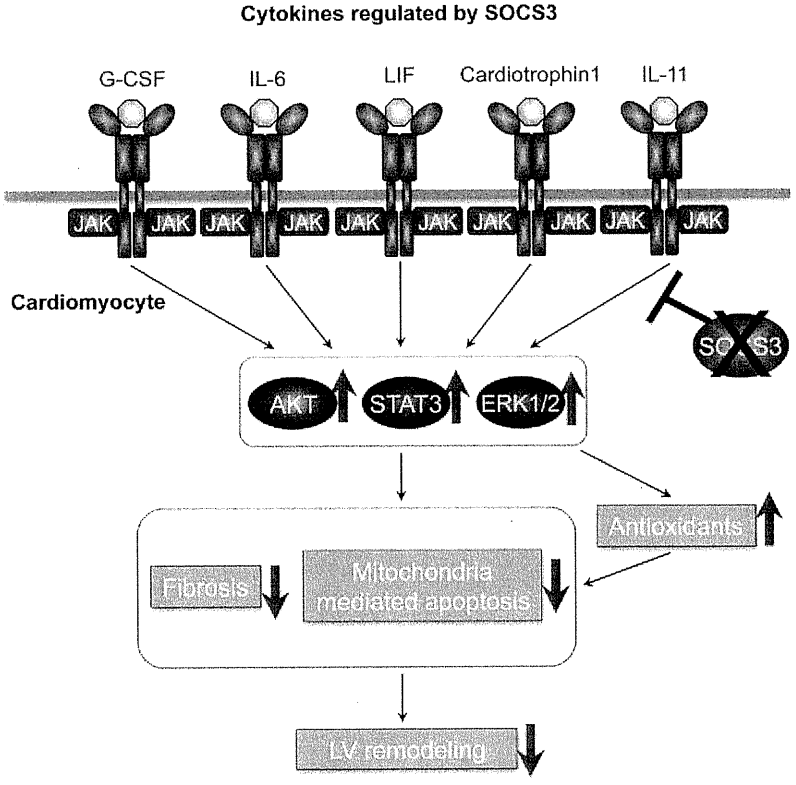

Figure 10 **Proposed Model for the Mechanism of Inhibition of LV Remodeling After AMI in Cardiac-Specific SOCS3-Deficient Mice**

Multiple JAK-STAT–activating cytokines including granulocyte colony-stimulating factor (G-CSF), leukemia inhibitory factor (LIF), cardiotrophin-1, interleukin (IL)-6, and IL-11 are induced in the ischemic myocardium after AMI. SOCS3 deletion in cardiomyocytes enhances cardioprotective signaling pathways including STAT3, AKT, and ERK1/2 pathways, which inhibit myocardial apoptosis by preventing mitochondria-mediated myocardial apoptosis and fibrosis and enhancing the expression of antioxidants, resulting in the prevention of LV remodeling after AMI. Abbreviations as in Figures 2 and 5.

Acknowledgments

The authors thank Dr. Kenneth Chien for generating SOCS3-flox mice. They also thank Kimiko Kimura, Miyuki Nishigata, Makiko Kiyohiro, and Miho Kogure for excellent technical assistance.

Reprint requests and correspondence: Dr. Hideo Yasukawa, Division of Cardiovascular Medicine, Department of Internal Medicine, Cardiovascular Research Institute, Kurume University School of Medicine, 67 Asahi-machi, Kurume 830-0011, Japan. E-mail: yahideo@med.kurume-u.ac.jp.

REFERENCES

1. Dorn GW 2nd. Novel pharmacotherapies to abrogate postinfarction ventricular remodeling. Nat Rev Cardiol 2009;6:283–91.
2. Mann DL. Mechanisms and models in heart failure: a combinatorial approach. Circulation 1999;100:999–1008.
3. Sutton MG, Sharpe N. Left ventricular remodeling after myocardial infarction: pathophysiology and therapy. Circulation 2000;101:2981–8.
4. Kehat I, Molkentin JD. Molecular pathways underlying cardiac remodeling during pathophysiological stimulation. Circulation 2010;122:2727–35.
5. Harada M, Qin Y, Takano H, et al. G-CSF prevents cardiac remodeling after myocardial infarction by activating the Jak-Stat pathway in cardiomyocytes. Nat Med 2005;11:305–11.
6. Minatoguchi S, Takemura G, Chen XH, et al. Acceleration of the healing process and myocardial regeneration may be important as a mechanism of improvement of cardiac function and remodeling by postinfarction granulocyte colony-stimulating factor treatment. Circulation 2004;109:2572–80.
7. Ueda K, Takano H, Niitsuma Y, et al. Sonic hedgehog is a critical mediator of erythropoietin-induced cardiac protection in mice. J Clin Invest 2010;120:2016–29.
8. Tada H, Kagaya Y, Takeda M, et al. Endogenous erythropoietin system in non-hematopoietic lineage cells plays a protective role in myocardial ischemia/reperfusion. Cardiovasc Res 2006;71:466–77.
9. Hirata A, Minamino T, Asanuma H, et al. Erythropoietin enhances neovascularization of ischemic myocardium and improves left ventricular dysfunction after myocardial infarction in dogs. J Am Coll Cardiol 2006;48:176–84.
10. Obana M, Maeda M, Takeda K, et al. Therapeutic activation of signal transducer and activator of transcription 3 by interleukin-11 ameliorates cardiac fibrosis after myocardial infarction. Circulation 2010;121:684–91.
11. Moon C, Krawczyk M, Ahn D, et al. Erythropoietin reduces myocardial infarction and left ventricular functional decline after coronary artery ligation in rats. Proc Natl Acad Sci U S A 2003;100:11612–7.
12. Bolli R, Dawn B, Xuan YT. Role of the JAK-STAT pathway in protection against myocardial ischemia/reperfusion injury. Trends Cardiovasc Med 2003;13:72–9.

13. Haghikia A, Stapel B, Hoch M, Hilfiker-Kleiner D. STAT3 and cardiac remodeling. Heart Fail Rev 2011;16:35–47.
14. Yamauchi-Takihara K. gp130-mediated pathway and heart failure. Future Cardiol 2008;4:427–37.
15. Barry SP, Townsend PA, Latchman DS, Stephanou A. Role of the JAK-STAT pathway in myocardial injury. Trends Mol Med 2007;13:82–9.
16. Fischer P, Hilfiker-Kleiner D. Survival pathways in hypertrophy and heart failure: the gp130-STAT axis. Basic Res Cardiol 2007;102:393–411.
17. Yasukawa H, Sasaki A, Yoshimura A. Negative regulation of cytokine signaling pathways. Annu Rev Immunol 2000;18:143–64.
18. Yasukawa H, Misawa H, Sakamoto H, et al. The JAK-binding protein JAB inhibits Janus tyrosine kinase activity through binding in the activation loop. EMBO J 1999;18:1309–20.
19. Sasaki A, Yasukawa H, Shouda T, Kitamura T, Dikic I, Yoshimura A. CIS3/SOCS-3 suppresses erythropoietin (EPO) signaling by binding the EPO receptor and JAK2. J Biol Chem 2000;275:29338–47.
20. Yasukawa H, Hoshijima M, Gu Y, et al. Suppressor of cytokine signaling-3 is a biomechanical stress-inducible gene that suppresses gp130-mediated cardiac myocyte hypertrophy and survival pathways. J Clin Invest 2001;108:1459–67.
21. Yasukawa H, Yajima T, Duplain H, et al. The suppressor of cytokine signaling-1 (SOCS1) is a novel therapeutic target for enterovirus-induced cardiac injury. J Clin Invest 2003;111:469–78
22. Yajima T, Yasukawa H, Jeon ES, et al. Innate defense mechanism against virus infection within the cardiac myocyte requiring gp130-STAT3 signaling. Circulation 2006;114:2364–73.
23. Yasukawa H, Ohishi M, Mori H, et al. IL-6 induces an anti-inflammatory response in the absence of SOCS3 in macrophages. Nat Immunol 2003;4:551–6.
24. Mori H, Hanada R, Hanada T, et al. Socs3 deficiency in the brain elevates leptin sensitivity and confers resistance to diet-induced obesity. Nat Med 2004;10:739–43.
25. Agah, R., Frenkel, P. A., French, B. A., Michael, L. H., Overbeek, P. A. & Schneider, M. D. J Clin Invest 1997;100:169–79.
26. Ikeuchi M, Matsusaka H, Kang D, et al. Overexpression of mitochondrial transcription factor a ameliorates mitochondrial deficiencies and cardiac failure after myocardial infarction. Circulation 2005;112:683–90.
27. Sano M, Schneider MD. Energizer: PGC-1 alpha keeps the heart going. Cell Metab 2005;1:216–8.
28. Tsutsui H, Kinugawa S, Matsushima S. Mitochondrial oxidative stress and dysfunction in myocardial remodelling. Cardiovasc Res 2009;81:449–56.
29. Ago T, Sadoshima J. Thioredoxin and ventricular remodeling. J Mol Cell Cardiol 2006;41:762–73.
30. Negoro S, Kunisada K, Fujio Y, et al. Activation of signal transducer and activator of transcription 3 protects cardiomyocytes from hypoxia/reoxygenation-induced oxidative stress through the upregulation of manganese superoxide dismutase. Circulation 2001;104:979–81.
31. Dawn B, Bolli R. HO-1 induction by HIF-1: a new mechanism for delayed cardioprotection? Am J Physiol Heart Circ Physiol 2005;289:H522–4.
32. Fujio Y, Kunisada K, Hirota H, Yamauchi-Takihara K, Kishimoto T. Signals through gp130 upregulate bcl-x gene expression via STAT1-binding cis-element in cardiac myocytes. J Clin Invest 1997;99:2898–905.
33. Hausenloy DJ, Yellon DM. Cardioprotective growth factors. Cardiovasc Res 2009;83:179–94.
34. Wegrzyn J, Potla R, Chwae YJ, et al. Function of mitochondrial Stat3 in cellular respiration. Science 2009;323:793–7.
35. Kang D, Kim SH, Hamasaki N. Mitochondrial transcription factor A (TFAM): roles in maintenance of mtDNA and cellular functions. Mitochondrion 2007;7:39–44.
36. Jung JE, Kim GS, Narasimhan P, Song YS, Chan PH. Regulation of Mn-superoxide dismutase activity and neuroprotection by STAT3 in mice after cerebral ischemia. J Neurosci 2009;29:7003–14.
37. Zhang X, Shan P, Jiang G, et al. Endothelial STAT3 is essential for the protective effects of HO-1 in oxidant-induced lung injury. FASEB J 2006;20:2156–8.
38. Okada H, Takemura G, Li Y, et al. Effect of a long-term treatment with a low-dose granulocyte colony-stimulating factor on post-infarction process in the heart. J Cell Mol Med 2008;12:1272–83.
39. Kobayashi H, Minatoguchi S, Yasuda S, et al. Post-infarct treatment with an erythropoietin-gelatin hydrogel drug delivery system for cardiac repair. Cardiovasc Res 2008;79:611–20.
40. Jacoby JJ, Kalinowski A, Liu MG, et al. Cardiomyocyte-restricted knockout of STAT3 results in higher sensitivity to inflammation, cardiac fibrosis, and heart failure with advanced age. Proc Natl Acad Sci U S A 2003;100:12929–34.
41. Najjar SS, Rao SV, Melloni C, et al. Intravenous erythropoietin in patients with ST-segment elevation myocardial infarction: REVEAL: a randomized controlled trial. JAMA 2011;305:1863–72.
42. Sakamoto H, Yasukawa H, Masuhara M, et al. A Janus kinase inhibitor, JAB, is an interferon-gamma-inducible gene and confers resistance to interferons. Blood 1998;92:1668–76.
43. Hamanaka I, Saito Y, Yasukawa H, et al. Induction of JAB/SOCS-1/SSI-1 and CIS3/SOCS-3/SSI-3 is involved in gp130 resistance in cardiovascular system in rat treated with cardiotrophin-1 in vivo. Circ Res 2001;88:727–32.

Key Words: acute myocardial infarction ▪ cytokine ▪ JAK-STAT ▪ left ventricular remodeling ▪ SOCS3.